Received: 2 January 2025 | Revised: 18 February 2025 | Accepted: 11 March 2025

DOI: 10.1002/pen.27193

RESEARCH ARTICLE

POLYMER ENGINEERING AND SCIENCE WILEY

Effect of printing orientation on mixed-mode fracture criterion of additively manufactured acrylonitrile butadiene styrene

Zhuoyuan Leng[1] | **Jun Li**[2] | **Vijaya B. Chalivendra**[1]

[1]Department of Mechanical Engineering, University of Massachusetts, North Dartmouth, Massachusetts, USA

[2]Department of Aerospace Engineering, Embry-Riddle Aeronautical University, Daytona Beach, Florida, USA

Correspondence
Vijaya B. Chalivendra, Department of Mechanical Engineering, University of Massachusetts, North Dartmouth, MA 02747, USA.
Email: vchalivendra@umassd.edu

Funding information
National Science Foundation, Grant/Award Number: NSF-CMMI-2438062

Abstract

This study presents an experimental investigation to examine the mixed-mode fracture behavior of fused filament fabrication printed acrylonitrile butadiene styrene (ABS). The single-edge notch bending specimen configuration is employed to perform mixed-mode fracture experiments. Four distinct printing orientations—90°, 0°, 45°/−45°, and 90°—are investigated. For each orientation, fracture studies are conducted under pure mode-I loading (symmetric three-point bending), mixed-mode I/II, and pure mode-II loading (asymmetric three-point bending) to establish a mixed-mode fracture criterion. The study evaluates the influence of printing orientation on fracture toughness, crack propagation behavior, and the mixed-mode fracture criterion. Scanning electron microscopy (SEM) is utilized to analyze the fracture surfaces and correlate the observed fracture mechanisms with the measured fracture toughness values. The findings reveal that printing orientation significantly affects both the fracture toughness and the mixed-mode fracture criterion. Among the orientations studied, the 90° specimens exhibit the highest fracture toughness and superior performance under all mixed-mode conditions. SEM images of the fracture surfaces across different printing orientations show the formation of smooth shear zones of varying sizes near the crack tip under mixed-mode and pure mode-II conditions. These zones suggest an enhanced resistance to crack propagation, with the degree of improvement differing among the orientations.

Highlights

- Mixed-mode fracture behavior of 3D-printed acrylonitrile butadiene styrene.
- Printing orientations have a major influence on mixed-mode fracture criterion.
- 90° printing orientation has the highest fracture toughness for mode-mixities.
- 0° printing orientation has the lowest fracture toughness for mode-mixities.
- Fracture surface has dominant shear zone for all mode-mixities except mode-I.

KEYWORDS

acrylonitrile butadiene styrene, additive manufacturing, fracture toughness, fusion deposition modeling, mixed-mode fracture criterion

1 | INTRODUCTION

Additive manufacturing (AM), particularly fused filament fabrication (FFF), has emerged as a revolutionary technology for fabricating complex geometrical shapes, offering notable advantages such as design flexibility, customization, reduced production costs, and minimized material waste.[1–5] FFF achieves these benefits through the layer-by-layer deposition of molten thermoplastic filaments, and this process has garnered extensive attention in various industries, including automotive, aerospace, and medical device manufacturing.[4,6] Among the thermoplastic materials employed in FFF, acrylonitrile butadiene styrene (ABS) distinguishes itself for its superior mechanical properties, ease of processing, and suitability for a diverse array of structural load-bearing applications. Nevertheless, despite its wide utilization, the mechanical properties of ABS processed by FFF are highly susceptible to a series of printing parameters, encompassing nozzle temperature, layer height, fill density, raster angle, and printing speed.[6–12] For instance, Rezaeian et al.[6] used different printing speeds to study the impact on the fracture properties of FFF-ABS specimens. The results demonstrate that, compared to other printing speeds, samples printed at 70 mm/s exhibit larger plastic deformation zones, enhanced filament bonding, and a reduced number of voids within the material. Consequently, these samples achieve higher tensile strength and fracture toughness.

The fracture toughness of FFF-printed ABS materials, especially under pure mode-I loading conditions, has been of great importance as the bonding between the printed layers is not strong and the cracks propagate along these weak planes.[13,14] McLouth et al.[15] investigated the influence of the printing direction on the fracture toughness of ABS. In their research, compact tension (CT) samples of ABS were printed in three orthogonal directions to analyze how the fracture toughness changes in accordance with the mesostructure. They discovered that when the alignment of the extruded filament layers shifted from parallel to perpendicular to the crack plane, the fracture toughness significantly increased by 54%. Hart et al.[16] employed SENB samples to study the effect of layer orientation on the fracture properties of ABS. Their study emphasized the considerable anisotropy of fracture toughness due to the laminated structure of FFF-ABS components. They compared the critical strain energy release rates for different crack tip/layer orientations and observed that the interlaminar fracture toughness was approximately one order of magnitude lower than the cross-layer toughness.

In practical structural applications, materials are commonly exposed to complex and combined loading conditions, including tensile, shear, and tear stresses. These circumstances often give rise to mixed-mode fracture scenarios, characterized by the simultaneous occurrence of mode-I (opening), mode-II (in-plane shear), and mode-III (out-of-plane shear) fracture mechanisms.[17] Comprehending and predicting the material behavior of FFF-printed plastics under these conditions are of paramount importance for the effective design and optimization of components in demanding environments.

Moreover, the complexity of mixed-mode fracture stems from the intricate interactions of fracture modes at the crack tip. Under these conditions, the path of crack propagation deviates from a straight trajectory due to the interaction of tensile and shear forces, often resulting in bending or irregularity, for example, sudden changes in the crack propagation direction and the presence of serrated or uneven surfaces along the crack path. This deviation could significantly influence the energy dissipation during the crack propagation process, thereby enhancing the material's fracture toughness and overall resistance to failure.[18–23] Furthermore, the direction of crack initiation and propagation is profoundly influenced by the degree of stress mixing. The crack does not always propagate along the direction of the maximum principal stress but follows a path determined by the combined stress state. This complicates the prediction of the crack propagation trajectory and leads to variations in the energy release rate at the crack tip.[24,25] Mixed-mode fracture plays an especially crucial role in composite and heterogeneous materials, particularly in interfacial failure. Weak interface bonding under mixed-mode stress conditions can lead to cracking, sliding, and delamination, all of which impact mechanical properties. Hence, improving interface bonding and enhancing fracture toughness constitute a key strategy for optimizing the mechanical properties of composite materials.[26]

Although a considerable amount of research has focused on the fracture behavior of ABS in pure mode-I conditions, research on its fracture toughness under mixed-mode loading conditions remains limited. Mode-I studies mainly examine tensile and opening stresses and typically overlook the complex interactions inherent in the shear mode in mixed-mode conditions.[27–29] Currently, there is a scarcity of research on mixed-mode loading in 3D-printed ABS materials, and most studies rely on a limited range of sample types and test configurations. Bahrami et al.[30] investigated the influence of printing orientation and raster angle on the fracture toughness of polycarbonate (PC) materials under mixed-mode conditions. Their results show that a raster angle perpendicular to the crack propagation direction significantly enhances fracture toughness by altering the crack path and increasing energy dissipation. Similarly, Nabavi-Kivi et al.[31] found that different printing speeds can affect several properties of FFF materials under mixed-mode conditions, such as tensile strength, elastic modulus, and J-integral. Ameri et al.[28,32] also utilized semicircular

bending (SCB) samples to investigate mixed-mode I/II loading in 3D-printed ABS; they plotted load–displacement curves, stress–strain curves, and crack angle figures, and the results indicated that cross-laminar failure could enhance fracture toughness. Their findings emphasize the role of layer interfaces in governing fracture behavior, in contrast to the behavior of traditional injection-molded ABS.

Likewise, Rajaee et al.[10] examined the impact of printing orientation on the mechanical performance of FFF-printed ABS, highlighting that fracture toughness varies significantly with layer alignment due to interfacial bonding characteristics. Their findings demonstrated that a 90° orientation exhibits the lowest fracture resistance due to weak interlayer adhesion, whereas a 0° orientation offers enhanced strength and toughness. Additionally, Syaefudin et al.[33] investigated the effect of raster angle on the fracture properties of FFF-printed ABS using the Essential Work of Fracture (EWF) approach. Their study revealed that transitioning from a 90° 5 layup to a 0° 5 layup increased fracture toughness by nearly 306%, while a ± 45° configuration provided a balance between energy dissipation and crack propagation resistance.

Fracture studies under pure mode-I and mixed-mode loading conditions have predominantly focused on determining fracture toughness values. However, the existing literature lacks comprehensive studies aimed at developing a mixed-mode fracture criterion that accounts for printing orientation and its influence on crack growth and fracture surface morphology. Establishing a fracture failure criterion under mixed-mode conditions is critical for determining safe mechanical loads when designing structures fabricated using Fused Filament Fabrication (FFF) with ABS materials that are subject to complex loading scenarios. Moreover, FFF inherently induces porosity within the materials for all printing orientations; understanding crack dynamics and relating them to the fracture criterion are essential for load-bearing applications. Hence, in this study, detailed mixed-mode fracture investigations are conducted on FFF-printed ABS materials with four distinct printing orientations, utilizing a SENB specimen configuration. The analysis extends beyond fracture toughness measurements to include post-failure examination of fracture specimens. Additionally, scanning electron microscopy (SEM) imaging is employed to analyze the fracture surfaces, providing deeper insights into the mixed-mode fracture behavior associated with various printing orientations. This research aims to fill the existing knowledge gap of understanding quantitative correlations of printing orientation with mixed-mode fracture toughness, thereby contributing to the optimization of FFF-printed ABS structures for enhanced fracture performance under mixed-mode loading conditions.

2 | MATERIAL AND PRINTING DETAILS

In this study, all samples are manufactured using an Ultimaker S5 3D printer based on the FFF. The 3D models of the samples are created and edited using Autodesk Inventor 2020 and then imported into Cura for setting the printing parameters. Cura converts the sample 3D models and the related printing parameters into G-code and transfers it to the 3D printer. According to the printing parameters, the printer first heats the nozzle and the build bed. Once they reach the specified temperature, the nozzle starts extruding the filament, and the printer begins printing layer by layer until the process is completed. A commercially available ABS filament from 3DXTECH of diameter 2.85 mm is fed into the printer at a constant rate. All specimens are printed on the horizontal plane with four different printing orientations of 45°/−45°, 90°, 0°/90°, and 0° as shown in Figure 1A.

The printing parameters used in this study are provided in Table 1, as suggested by the printer manufacturer for optimum performance. Tests are also performed at different printing speeds to justify the values, using the 90° printing orientation as a reference case. The results indicated that within the 45–65 mm/s range, the fracture performance of the printed specimens remained relatively the same with no significant differences in fracture toughness. However, at lower printing speeds, excessive heat accumulation led to overmelting of the filament, which in turn caused irregular extrusion flow and distortion in the printed layers, thereby affecting interlayer bonding quality. Conversely, at higher printing speeds, insufficient bonding time between layers resulted in reduced interfacial adhesion, leading to increased void formation and interlayer defects, which negatively impacted the fracture toughness.

3 | EXPERIMENTAL DETAILS

3.1 | Quasi-Static fracture loading

This study uses a three-point bending test method to test single-edge notch bending (SENB) samples under pure mode-I, mixed-mode, and pure mode-II conditions, as shown in Figure 1B,C. Pure mode-I (opening mode) is applied using the same distances between the left and right rollers (S_1 and S_2). To apply a mixed-mode condition to the specimen, the distance between S_1 and S_2 is varied for different mode-mixities, and this adjustment alters the ratio of tensile to shear deformation.[26,31] Mixed-mode condition is related to different S_1/S_2 ratios, as the contribution of shear mode and opening mode at the crack tip varies with the change in the S_2 distance

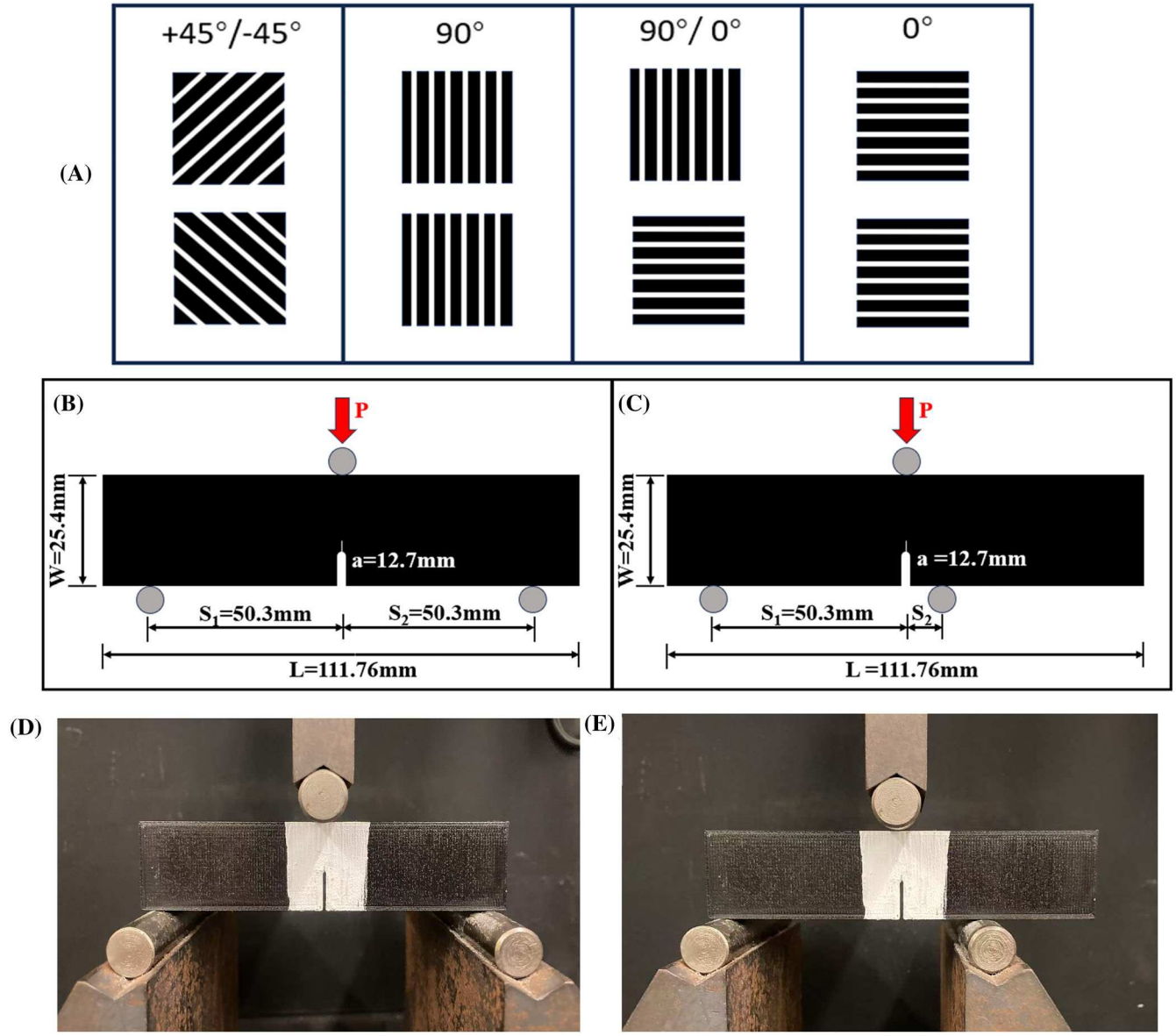

FIGURE 1 (A) Printing Orientations used in this study, (B) geometry and loading condition of the SENB specimen for pure mode-I fracture, and (C) geometry and loading condition of the SENB specimen for mixed-mode I/II and pure mode-II fracture, where the values of S_2 vary with mode mixity and are provided in Table 2. (D) Actual testing setup under pure mode-I condition. (E) Actual testing setup under mixed-mode condition.

where S_1 is kept constant. For pure mode-II conditions, the right roller is placed very close to the crack (S_2 is very small), where the in-plane shear stress becomes more significant compared to bending. In all cases, the three-point bending is performed at a constant crosshead displacement of 5 mm/min by using an INSTRON 5569 loading device. The size of the test specimen is 111.76 × 25.4 × 12.7 mm^3 with an 11.7 mm initial notch according to ASTM D5045 standard. A 1 mm precrack is created at the notch tip by using a sharp razor blade and a small hammer. The load–displacement diagrams obtained for all mixed-mode conditions are processed to determine the mixed-mode I/II fracture toughness and fracture criterion. The mode-I and mode-II stress intensity factors (K_I and K_{II}) are calculated by using the equations (1–3). The load (P) is related to the crack initiation point determined using a real-time video image taken during the testing. A MicroCapture® Pro digital microscope is used at a framing rate of 30 fps to monitor crack initiation and propagation. The video recording and the application of loading are started simultaneously with no time lag. Later, these measurements are correlated to make plots discussed in the below sections.

TABLE 1 Printing parameters.

Printing parameters	Values
Printing plane	XY flat
Nozzle diameter	0.4 mm
Extrusion temperature	255°C
Bed temperature	115°C
Layer height	0.2 mm
Infill density	100%
Printing speed	50 mm/s
Ambient temperature	23 ± 2°C
Humidity	45 ± 5%

$$K_I = \sigma\sqrt{\pi a}Y_I, \tag{1}$$

$$K_{II} = \sigma\sqrt{\pi a}Y_{II}, \tag{2}$$

$$\text{where } \sigma = \frac{6PS_1S_2}{tW^2(S_1+S_2)} \tag{3}$$

where Y_I and Y_{II} are the mode-I and mode-II geometry factors, t is the thickness of the sample, and W is the width of the sample.[34] For pure mode-I and mode-II conditions, the above equations (1) and (2) provide critical stress intensity factors K_{Ic} and K_{IIc}, respectively.

For mixed-mode fracture conditions, the loading point distances ($2S_1/L$ and $2S_2/L$) used in Figure 1C and geometry factors (Y_I and Y_{II}) used in equations (1) and (2) for different mode-mixities (as defined in the equation (4)) are shown in Table 2 obtained from Aliha et al.[34]

$$M^e = \frac{2}{\pi}\tan^{-1}\left(\frac{K_I}{K_{II}}\right) \tag{4}$$

3.2 | Scanning electron microscopy (SEM)

To further investigate the impact of different mode-mixity and various printing orientations on crack surface, a Zeiss Sigma VP field emission scanning electron microscope (FE-SEM) is employed to study and compare the microstructure of the fracture surfaces of the samples. The FE-SEM is operated at a voltage range of 3 kV–5 kV, with a working distance range of 6–9 mm, and at a magnification range of 100× ∼ 50,000×. The tested samples are cut into small sections that include the entire fracture surface and are set on a modified 50-mm-diameter stub using conductive double-sided tape. In this study, all images are captured under 0.5 kV.

4 | RESULTS AND DISCUSSION

4.1 | Pure mode-I and mode-II Fracture toughness

Figure 2 presents both the pure mode-I and mode-II fracture toughness values (K_{Ic} and K_{IIc}) for all printing orientations (90°, 45°/−45°, 0°, and 90°/0°). The error bars are determined using student t-distribution at 95% confidence limits, which accounts for the standard deviation and the number of test specimens tested for each orientation. At least five samples are tested for each printing direction, and outliers are eliminated. Except for the 0° orientation, the differences in mode-I and mode-II fracture toughness are significantly different, as indicated by the nonoverlapping error bars. It is interesting to notice that the bond strength between the printed filaments for the 0° orientation offered almost similar resistance to initiate the crack under both pure mode-I and mode-II loading conditions. For the 90° printing orientation, it demonstrates the highest average fracture toughness among all configurations under mode-I fracture. This enhanced fracture resistance can be attributed to the direction of applying bending loads with respect to the filament structure. Specifically, the stress is transversely transferred throughout the entire filament, compelling any expanding cracks to traverse the cross-section of the filament, a phenomenon known as cross-layer cracking, as shown in Figure 3 (A1), and the SEM image of Figure 3 (A2) substantiates this phenomenon and presents a smooth cross-layer fracture surface. This is because the cracks propagate normal to the direction of tensile stress, typically without prominent shear or frictional forces, leading to a relatively smooth fracture surface. The energy requirement for cross-layer cracking is extremely high as it needs to overcome the internal cohesion within each filament, thereby leading to greater fracture energy. For mode-II fracture, the 90° orientation also exhibits the highest average fracture toughness. Based on the crack trajectory observed in the failed specimens under mode-II loading, the crack initially follows a curved path after initiation (as shown in Figure 3 (B1)), while the overall trend remains similar to that of mode-I fracture. This phenomenon is further validated by the SEM image of Figure 3 (B2), where the fracture surface near the crack tip is no longer entirely smooth and uniform, but instead displays distinct surface gradients. These gradients indicate that the crack propagation mechanism involves significant shear deformation rather than direct tensile separation. Furthermore, due to interlayer debonding and frictional resistance along the crack path, shear-dominated fracture requires additional energy dissipation. Additionally, the relatively weak interlayer bonding at 90° results in the crack propagating laterally through the structure rather

TABLE 2 Corresponding values of ABS SENB samples under mixed-mode conditions.

Mode-mixity (M^e)	$M^e = 1$ (Pure mode-I)	$M^e = 0.8$	$M^e = 0.6$	$M^e = 0.4$	$M^e = 0.2$	$M^e = 0$ (Pure mode-II)
$2S_1/L$	0.9	0.9	0.9	0.9	0.9	0.9
$2S_2/L$	0.9	0.14	0.0875	0.065	0.045	0.03
Y_I	1.49	1.21	1.00	0.82	0.47	0.0
Y_{II}	0.00	0.39	0.75	1.07	1.63	2.48

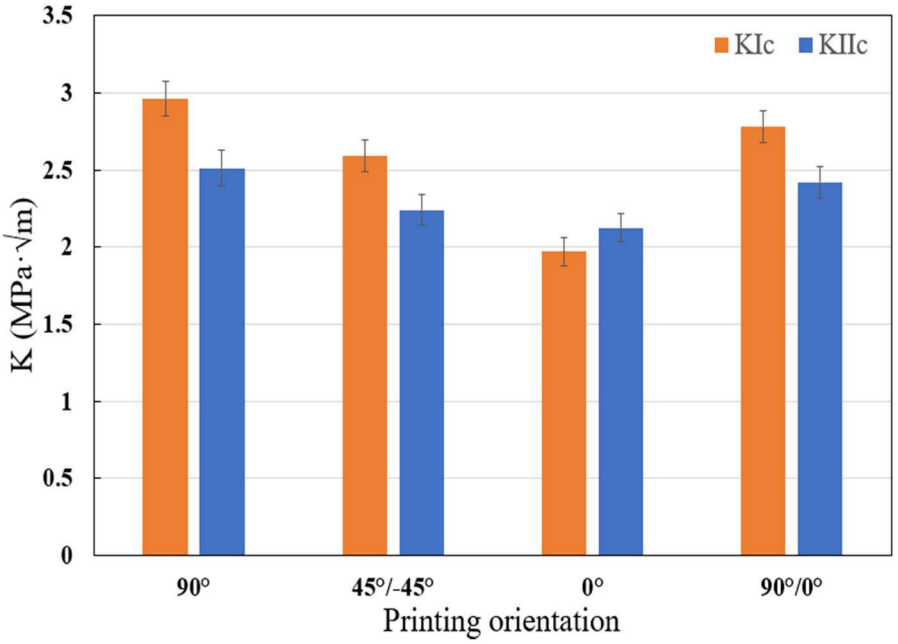

FIGURE 2 Mode-I and mode-II fracture toughness of different printing orientations.

than directly penetrating individual filaments. This lateral propagation mode implies that the crack must overcome substantial interlayer bonding forces and internal cohesion within the filaments as it propagates. Consequently, compared to other printing orientations, crack propagation in this configuration necessitates higher energy consumption, leading to greater energy dissipation and, consequently, higher fracture toughness.

Conversely, the 0° orientation shows the lowest average fracture toughness for both mode-I and mode-II conditions, suggesting that the alignment of cracks with the filament orientation (shown in Figure 1A) needs less resistance for the initiation of the crack. In this situation, the crack extends along the length of the filaments, typically advancing through the interlayer interfaces rather than severing individual filaments, as shown in Figure 4 (A1). The SEM image (shown in Figure 4 (A2)) also demonstrates that the cracks indeed extended along the length of the filaments, revealing a mechanism dominated by interlaminar delamination. Compared with the cross-layer crack propagation observed in the 90° orientation, the energy required for interlaminar cracking is significantly lower, as it mainly involves the delamination of the interface between consecutive layers rather than the disruption of the structural integrity of the filaments themselves. This distinction explains why the 0° orientation exhibits the lowest average fracture toughness among all configurations. Under mode-II loading, the fracture surface exhibits a pronounced shearing zone at the crack tip, as shown in Figure 4 (B2), suggesting that crack propagation involves a combination of filament slip and plastic deformation before ultimate shear failure. Despite the relatively weak interlayer adhesion, the material exhibits notable resistance due to frictional and cohesive interactions acting along the shear plane. This explains why the K_{IIc} value for the 0° orientation is greater than the K_{Ic} value, indicating that these specimens can withstand higher shear stresses than tensile stresses. Nevertheless, compared to other orientations, the overall fracture toughness of the 0° orientation remains relatively low under mode-II loading. As illustrated in Figure 4 (B1), the crack trajectory remains consistent with mode-I, yet the SEM image in Figure 4 (B2) reveals a key distinction with a prominent shearing zone at the crack tip.

The 90°/0° specimens lie between the 90° and 0° printing orientations, leading to a fracture toughness value that

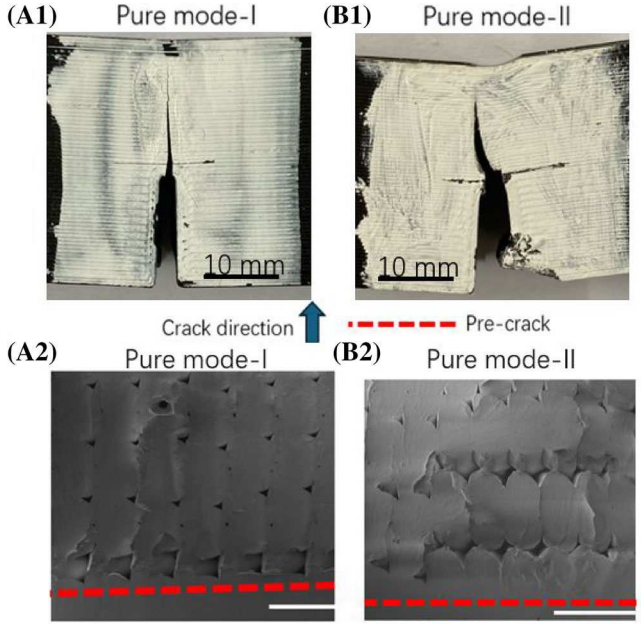

FIGURE 3 Images of 90° printing orientations: Crack propagation path under (A1) pure mode-I loading, (B1) pure mode-II loading. SEM image of the fracture surface under (A2) pure mode-I loading, (B2) pure mode-II loading. The scalar bars (white line) shown in the SEM images are 500 μm. The red dotted lines in SEM images represent the precrack positions before the crack initiation.

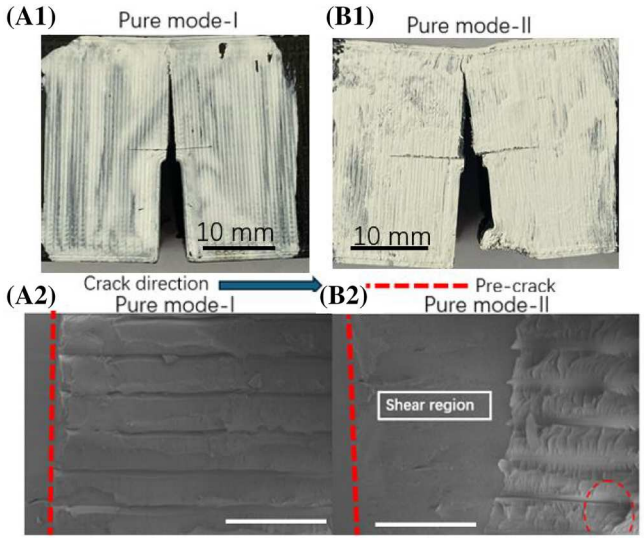

FIGURE 4 Images of 0° printing orientations: Crack propagation path under (A1) pure mode-I loading, (B1) pure mode-II loading. SEM image of the fracture surface under (A2) pure mode-I loading, (B2) pure mode-II loading. The scalar bars (white line) shown in the SEM images are 500 μm. The red dotted lines in SEM images represent the precrack positions before the crack initiation.

lies between those observed for the pure 90° and 0° orientations. This configuration gives rise to a more intricate crack path that navigates between the interlayer and

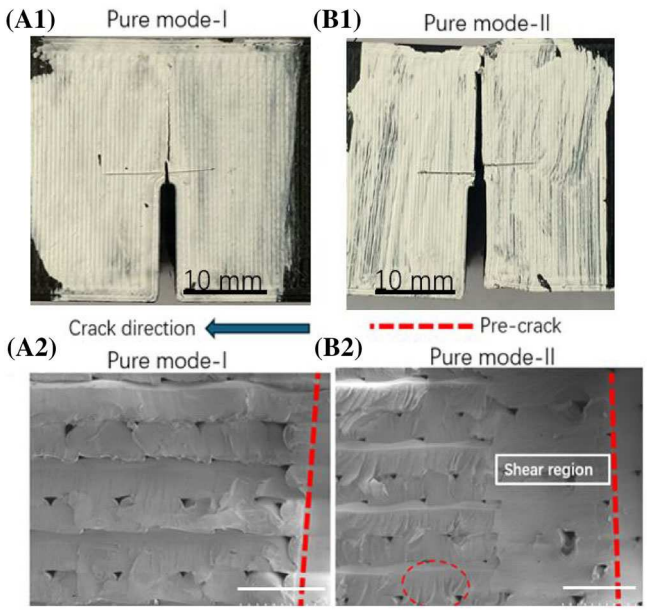

FIGURE 5 Images of 45°/-45° printing orientations: Crack propagation path under (A1) pure mode-I loading, (B1) pure mode-II loading. SEM image of the fracture surface under (A2) pure mode-I loading, (B2) pure mode-II loading. The scalar bars (white line) shown in the SEM images are 500 μm. The red dotted lines in SEM images represent the precrack positions before the crack initiation.

translaminar regions, as shown in Figure 5 (A1). Initially, the extending crack looks for the lower-energy interlayer paths parallel to the filament orientation, which is a characteristic of the 0° region, thereby facilitating crack propagation. However, as the crack traverses different parts of the material, it eventually encounters translaminar sections that demand more energy for propagation, as is the case in the 90° orientation. The combination of interlayer and translaminar propagation paths results in a moderate fracture toughness, reflecting a balance in the resistance to crack initiation and growth. As depicted in Figure 5 (A2), both the interlayer and the translaminar regions can be noticeably observed. Due to the differences in energy dissipation between these two mechanisms, a slight variation in fracture timing occurs, producing a partially uneven fracture surface at the transition zones. This variation contributes to the observed gradients in the fracture morphology, reinforcing the mixed-mode nature of the failure process. Under mode-II conditions, the fracture toughness of the 90°/0° configuration still lies between that of the pure 0° and 90° orientations, confirming the influence of mixed fracture mechanisms. The crack propagation mechanism is the same as in mode-I, being a mixture of interlayer sliding and cross-layer failure. However, as indicated in Figure 5 (B1), the initial crack tip will initiate and propagate along a straight line for a short distance; then, the

filaments will deform under the influence of shear stress, presenting the same lateral development as in the 90° orientation. Subsequently, as the stress exceeds the critical point, the crack extends along the weaker interlayer region, exhibiting the characteristics of the 0° orientation. The shear zone observed in Figure 5 (B2) and the characteristics of the fracture surface integrating both 90° and 0°, such as gradients and relatively rough fracture surfaces (indicated by a red ellipse), also validate the aforementioned analysis. In regions where crack propagation occurs through interlayer delamination, the energy required is relatively low, resulting in smoother fracture surfaces. Conversely, as the crack transitions into translaminar propagation, the fracture surface becomes increasingly rough and irregular, indicative of higher energy absorption. This variation in fracture morphology correlates with the measured fracture toughness values, as the alternating crack paths introduce localized variations in resistance, ultimately contributing to an intermediate toughness level. Furthermore, as the crack advances, localized plastic deformation within the filaments enhances energy dissipation, further supporting the observed fracture toughness trend. However, a key distinction between the 90°/0° and pure 90° specimens is the absence of an initial curvature in the crack path, as evident in Figure 5 (B1). This can be attributed to the predominant alignment of the crack either parallel (0°) or perpendicular (90°) to the filament orientation, which restricts the crack from deviating into a curved trajectory. SEM imaging further reveals that in the 90°/0° specimens, the crack front encounters localized resistance from the 0° filaments, which act as structural barriers. These filaments impose an obstruction that prevents the crack from extending laterally in the weak plane of the 90° filaments, limiting the influence of shear-induced deflection.

For the 45°/−45° printing orientation, the average mode-I fracture toughness is marginally lower than that of the 90°/0° orientation. The alternating layer structure at 45° and −45° angles gives rise to a complex stress distribution under mode-I loading. In this orientation, cracks are compelled to traverse the interlayer interfaces and filament cross-sections, thereby generating a mixed crack propagation path (shown in Figure 6 (A1)). Although the 45°/−45° orientation exhibits a certain resistance to crack propagation due to the requirement for cracks to pass through different filament layers, the energy needed for the initiation of propagation is lower than that of the 90° orientation. This is mainly attributed to the mixed directionality and the presence of weaker planes along the interface boundaries. As the analysis of the SEM image shown in Figure 6 (A2) reveals, for the direction where filament breakage is not necessary, only a portion in the middle (indicated by blue ellipse) presents the characteristics of the fracture surface, while voids exist in other positions except those showing

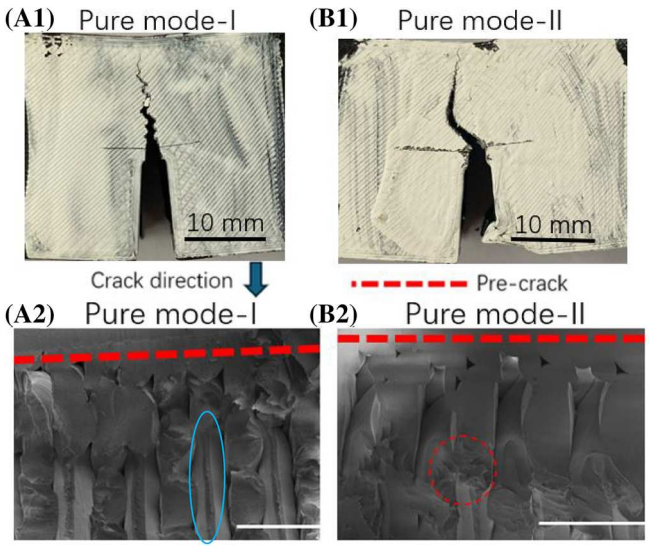

FIGURE 6 Images of 90°/0° printing orientations: Crack propagation path under (A1) pure mode-I loading, (B1) pure mode-II loading. SEM image of the fracture surface under (A2) pure mode-I loading, (B2) pure mode-II loading. The scalar bars (white line) shown in the SEM images are 500 μm. The red dotted lines in SEM images represent the precrack positions before the crack initiation.

fracture characteristics, resulting in a reduction in fracture toughness. In mode-II fracture, as can be seen from Figure 6 (B1), under the action of shear stress, the angle of the 45°/−45° crack path is significantly smaller than 45° and exhibits a curved extension with the angle gradually decreasing in the latter half, gradually evolving into a straight line. The SEM image in Figure 6 (B2) provides critical insights into the failure mechanisms contributing to the lower mode-II fracture toughness of the 45°/−45° orientation. A distinct shear zone at the crack tip indicates significant filament bending and localized plastic deformation before failure. This gradual shear strain accumulation suggests initial resistance to crack propagation, followed by failure as stress concentrations exceed filament strength. The presence of this shear zone underscores the material's tendency toward localized shearing rather than abrupt fracture, impacting energy dissipation and fracture toughness. Additionally, SEM observations reveal larger voids near the fracture surface, likely due to incomplete filament fusion and weak interlayer adhesion. These voids act as stress concentrators, facilitating premature crack propagation and reducing stress transfer efficiency. As a result, localized failure occurs, diminishing the material's resistance to shear stress and lowering its mode-II fracture toughness. Furthermore, distinct tearing marks (highlighted in Figure 6 (B2)) indicate a progressive failure process driven by shear stress, where filament stretching and partial separation precede complete rupture. This gradual shearing process dissipates

less energy than cohesive filament failure, aligning with the measured reduction in fracture toughness.

Over all, under pure mode-I, crack propagation occurs in such a way that the extension angle coincides with the initial crack direction, and the crack propagation direction remains perpendicular to the applied load for all printing orientations. This condition ensures that the sole stress component in the crack propagation direction is the opening stress, allowing for a relatively straightforward and uniform stress distribution at the crack tip. Hence, the crack follows a straight path, and the perturbation to the surrounding material is minimal. In pure mode-I, no shear stress acts in the direction of crack propagation; hence, the crack propagation angle of materials with diverse mechanical properties remains approximately zero, resulting in consistent crack paths that are essentially unperturbed by the anisotropy introduced by different printing orientations.

In contrast, in pure mode-II loading, the sliding or in-plane shear mode predominates. The shear stress in mode-II induces significant deformation at the crack tip, resulting in alterations in the stress field prior to any observable crack extension. This fracture mode involves complex stress interactions, leading to nonlinear crack paths, although the overall direction of the principal crack remains consistent with the initial crack direction in mode-I. Further analysis, particularly via SEM, can offer deeper insights into the fracture mechanisms associated with mode-II. SEM images reveal a distinct shear region at the crack tip, which is a characteristic indication of the influence of the sliding mode. The presence of this shear region suggests that the material has encountered and overcome substantial resistance, as evidenced by the internal filaments undergoing slip, deformation, and ultimately shear failure. The filament fracture patterns beyond the shear region are also clearly discernible, and in comparison to mode-I, the fracture surfaces are rougher. After a certain extent of crack propagation, the crack opening of the sample widens, which enables the tensile stress state at the crack tip to regain its dominance. Hence, even under conditions dominated by mode-II, the latter part of the crack still tends to propagate along the initial crack direction, as depicted in (b1) of Figures 3–6.

4.2 | ixed-mode I/II fracture toughness for different printing orientations

Figure 7 depicts the variations of the stress intensity factors for mode-I and mode-II as a function of the mode-mixity. The x-axis represents the mode-mixity, ranging from 0 to 1, where 0 indicates pure mode-II loading, and 1 represents pure mode-I loading. The graph incorporates curves for four different printing orientations (0°, 45°/−45°, 90°/0°, and 90°), represented by distinct symbols (such as circles, squares, triangles, and rhombuses). The orange curves represent the K_I variation, whereas the blue curves represent the variation of K_{II}.

As the mode-mixity increases from 0 to 1, the K_I values generally exhibit an increasing trend across all printing orientations. At a mode-mixity of 1 (pure opening mode loading), the K_I values attain their maximum. As the mode-mixity increases from 0 to 1, the slope of increase of K_I for different printing orientations is similar initially; however, beyond $M^e = 0.2$, the slope varies significantly. The values of K_I follow the same pattern for each printing orientation independent of applied mode-mixity, where the 90° orientation always has the highest K_I and the 0° orientation has the lowest K_I. However, the slope of decline of K_I is very high for the 90° orientation compared to other orientations when the mode-mixity changes from 0.6 to 0.2.

When the mode-mixity approaches 0, the K_{II} values reach the peak, suggesting that the loading is pure shear mode. Similar to K_I, the variation of K_{II} also depends on the printing orientation. The differences indicate that certain printing orientations are more conducive to generating higher shear stress intensities. Overall, the pattern of K_{II} follows a similar trend to that of K_I, where the 90° orientation always has the highest K_{II} and the 0° orientation has the lowest K_{II} for most of the mode-mixities.

For the 0° orientation, cracks are more likely to approach the fracture mode typically characterized by interlaminar fracture irrespective of the applied mode-mixity, as depicted in Figure 8A. This is due to the fact that the cracks follow a path that has minimum resistance, leading to behavior tending toward the pure fracture mode.

This behavior is mainly because interlaminar fracture requires less energy for initiation and propagation, making it an energetically favorable path under mixed-mode conditions. This can be evidenced in the SEM shown in Figure 8B, where it is demonstrated that the shear zone changes accordingly as the mode-mixity gradually varies. Although the length of the shear zone increases from mode-mixity of 0.8 to 0.6, the fracture surface beyond the shear zone is similar. The closer it approaches pure mode-II, the larger the shear zone becomes, as noticed in mode-mixity = 0.2. Moreover, the subsequent fracture surface does not undergo overly significant changes, except for alterations in roughness (red circle) with a decrease in mode-mixity due to the shearing of the crack front before failure.

For 90° samples under mixed-mode conditions, the propagation of cracks becomes more complex. The trajectory is no longer a straight line but a curved path that dynamically adapts to the stresses around the crack tip. As depicted in Figure 9A, the extent of curvature in the crack propagation path increases with the reduction of the mode-mixity. This phenomenon can be understood in

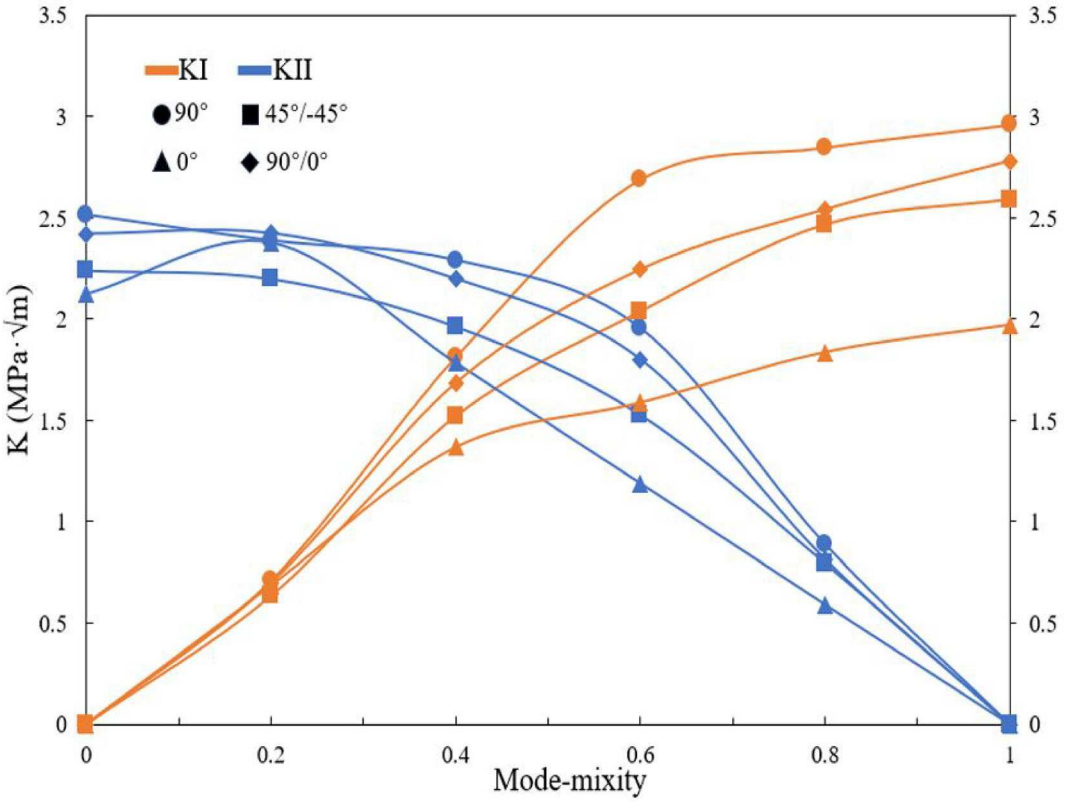

FIGURE 7 The variation of mode-I and mode-II fracture toughness as a function of mode-mixity for all four printing orientations.

the SEM image of the crack fracture surface (shown in Figure 9B). This complexity is obviously evident in the SEM images of the crack fracture surface, which reveal a distinct gradient along the fracture with no shear zone due to the presence of filament ahead of the crack tip. The initial crack has to break the filament ahead to initiate and propagate further. At mode-mixity of 0.8, the fracture surface is almost similar to mode-I with no gradient. The presence of a gradient can be noticed with a further decrease in mode-mixity to 0.6. The gradient indicates the varying degrees of the mixed fracture mode in different regions of the crack. This mixed-mode behavior implies that the crack propagates through double fracture mechanisms simultaneously, leading to an uneven fracture surface while shearing of the filament ahead of the crack tip, as predominantly evident at the mode-mixity of 0.2. When the crack extends horizontally and generates a gradient on the fracture surface, its underlying principle is similar to that of the 0° orientation. The formation of this gradient implies that certain regions of the crack encounter conditions that require less energy for crack extension. These regions tend to adopt behavior similar to the opening mode, thereby maximizing the total energy savings. This phenomenon emphasizes that despite the complex interactions existing in mixed-mode fracture, the crack often adjusts its path to follow the direction with the lowest energy demand. By doing so, it ensures the optimal balance between resistance and the energy required for further propagation, ultimately shaping the trajectory of the fracture surface.

As presented in Figures 10A and 11A, although the 90°/0° specimens demonstrated a crack propagation direction trend closer to that of the 0° samples (with the crack propagation direction remaining vertical as the mode-mixity varies), and the 45°/−45° samples displayed a trend more similar to that of the 90° samples (with the crack propagation direction becoming increasingly curved as the mode-mixity changes), analogous tendencies were observed in the SEM images of the fracture surfaces of both (as shown in Figures 10B and 11B). The images evidently indicate the presence of extensive shear deformation along the crack path, particularly at lower mode-mixity for both 90°/0° and 45°/−45°specimens. Interestingly, the shear zone for the 45°/−45°samples is significantly shorter compared to the 90°/0° case as the initial crack experiences the crossed filaments of 45°/−45° ahead before the initiation and propagation and breaks one of the filaments. However, the fracture surfaces of both these orientations exhibit pronounced unevenness and tearing marks (red circles) that vary with the mode-mixity, suggesting that the crack encountered different magnitudes of shear stress during its propagation. The SEM images of the fracture surfaces of

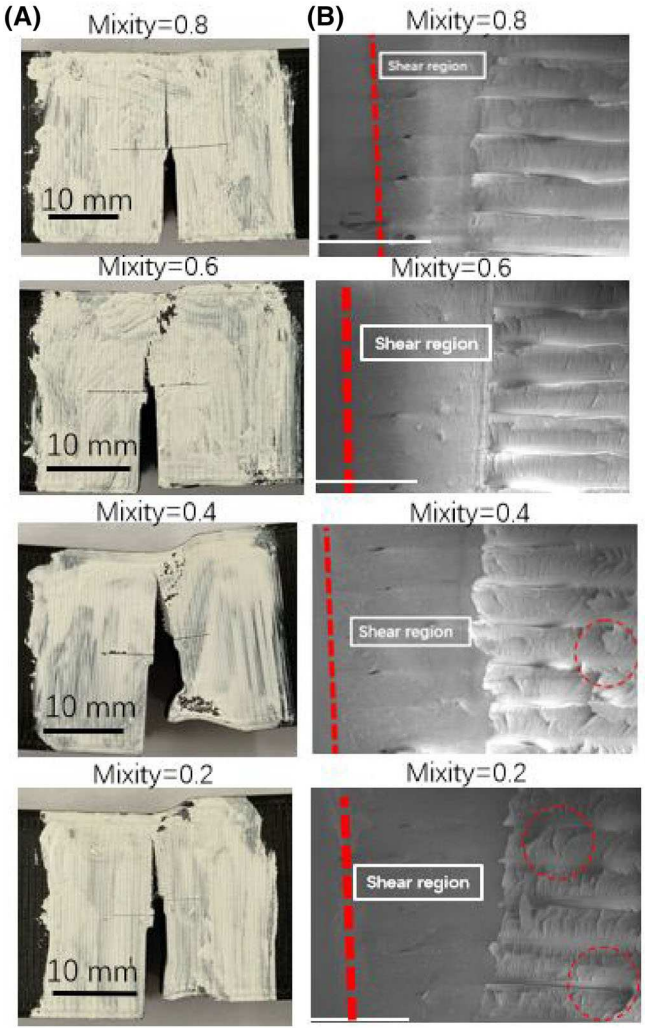

FIGURE 8 Images of crack propagation direction and SEM of crack surfaces of 0° printing orientation under mixed-mode loading conditions. (A) Crack propagation direction for all mixed-mode loading conditions, (B) SEM of crack surfaces for all mixed-mode loading conditions, and the scalar bar (white line) in the SEM is 500 μm.

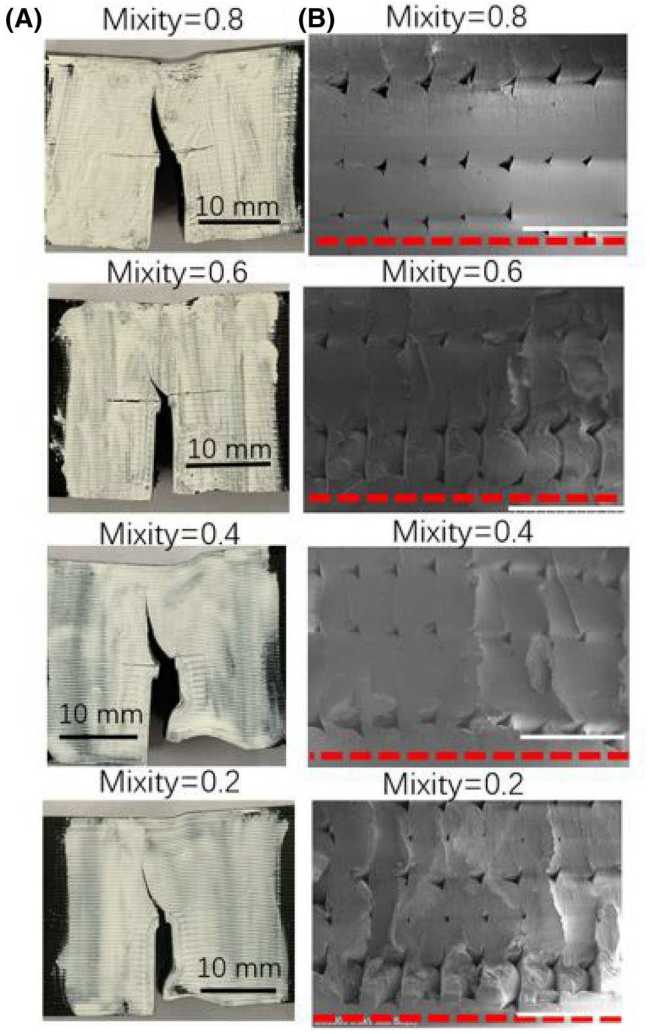

FIGURE 9 Images of crack propagation direction and SEM of crack surfaces of 90° printing orientation under mixed-mode loading conditions. (A) Crack propagation direction for all mixed-mode loading conditions, (B) SEM of crack surfaces for all mixed-mode loading conditions, and the scalar bar (white line) in the SEM is 500 μm.

both reveal that these regions concurrently possess the characteristics of brittle (tensile) and ductile (shear) mechanisms, supporting the notion that both forces facilitate crack initiation for propagation. The mixed-mode fracture results in a rough surface morphology, with distinct shear zones observable at lower mode-mixity, reflecting the predominance of shear stress. This behavior emphasizes the dynamic adaptation of the crack path to the evolving local stress field around the crack tip.

4.3 | Mixed-mode I/II fracture criteria for different printing orientations

The mixed-mode fracture criterion can be represented in a general form as given in the below equation[35]:

$$\left(\frac{K_I}{K_{Ic}}\right)^{\alpha}+\left(\frac{K_{II}}{K_{IIc}}\right)^{\beta}=1 \tag{5}$$

α and β denote the contribution of different mode of cracks to the fracture of the material and are empirical constants related to the material characteristics. For example, when α and β are equal to 1, this implies that the mode-I and mode-II have a linear relationship. This situation indicates that the initiation and propagation of cracks will rely on the superposition of these two modes, and the contribution weights of both to the crack initiation are equal. This is applicable to those materials whose microstructures are relatively uniform in all directions,[36] without obvious anisotropy or specific strengthening/weakening phenomena of a particular mode. When $\alpha>1$ and $\beta=1$, the contribution of the stress intensity factor of

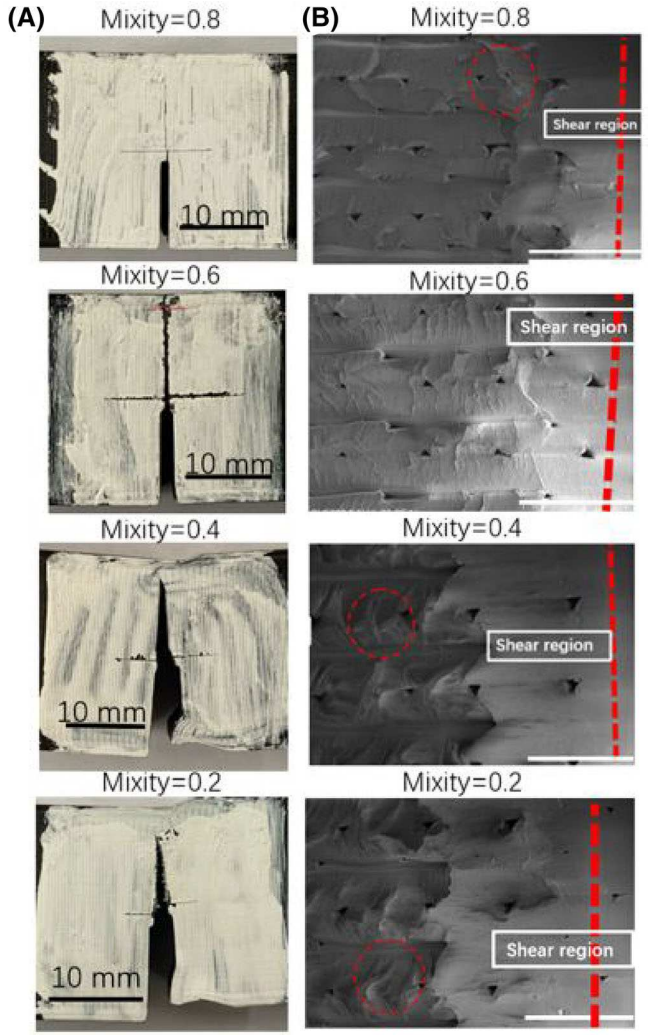

FIGURE 10 Images of crack propagation direction and SEM of crack surfaces of 90°/0° printing orientation under mixed-mode loading conditions. (A) Crack propagation direction for all mixed-mode loading conditions, (B) SEM of crack surfaces for all mixed-mode loading conditions, and the scalar bar (white line) in the SEM is 500 μm.

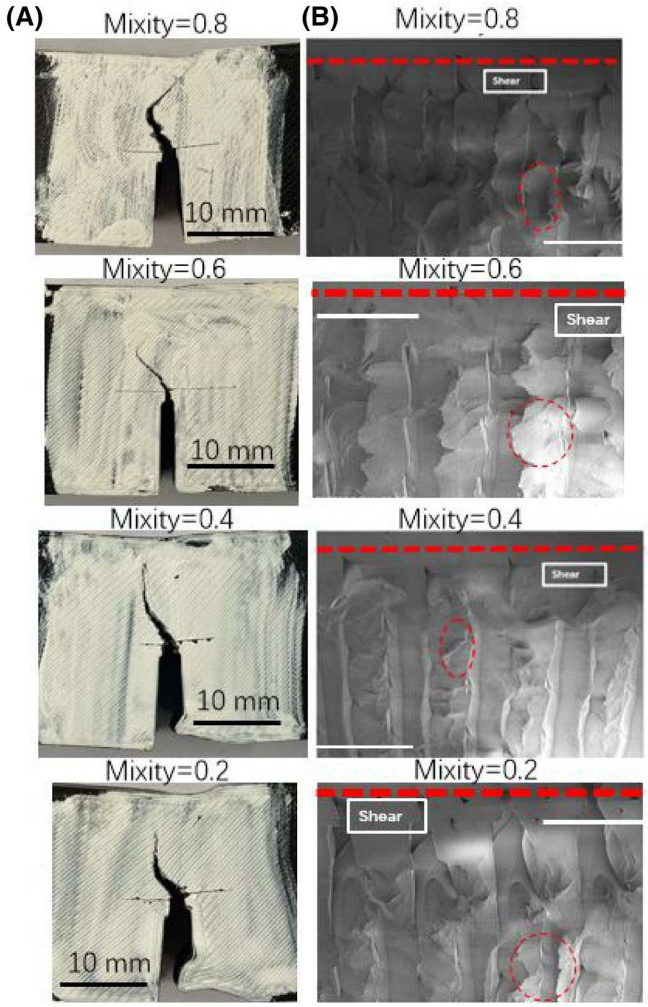

FIGURE 11 Images of crack propagation direction and SEM of crack surfaces of 45°/−45° printing orientation under mixed-mode loading conditions. (A) Crack propagation direction for all mixed-mode loading conditions, (B) SEM of crack surfaces for all mixed-mode loading conditions, and the scalar bar (white line) in the SEM is 500 μm.

the openning mode in the mixed-mode fracture criterion will increase. This implies that the material has greater resistance to the opening mode and a higher $\left(\frac{K_I}{K_{Ic}}\right)$ is required to initiate the crack. When $\alpha < \beta$, this suggests that the fracture resistance of the material is more sensitive to the shearing mode, and a higher $\left(\frac{K_{II}}{K_{IIc}}\right)$ value is needed to reach the critical condition for crack initiation.

The calculated mode-I and mode-II stress intensity factors for different mode-mixities shown in Figure 7 are used to determine the ratio of $\left(\frac{K_I}{K_{Ic}}\right)$ and $\left(\frac{K_{II}}{K_{IIc}}\right)$ and plotted in Figure 12. Later, the curve fitting was used to determine α and β values given in equation (5). The determined emperical constants α and β for different printing orientations are provided in Table 3. These parameters are helpful to know the dominance of mode-I or mode-II contributions for initating the crack under mixed-mode conditions.

For 90° orientation, the parameters are $\alpha = 2.3$ and $\beta = 3.3$, which are relatively high values suggest that this orientation exhibits significant resistance to shearing mode. In case of 45°/−45° orientation, the parameters are $\alpha = 1.9$ and $\beta = 2.1$, which are lower than the 90° samples. This indicates that this orientation has weaker fracture resistance and resistance for shearing mode is slightly higher than the opening mode. For 0° direction, the parameters are $\alpha = 1.7$ and $\beta = 1.5$. The lower β value indicates that the material's resistance for the shear mode failure load is less for this orientation. For 90°/0° samples, the parameters are $\alpha = 2.5$ and $\beta = 2.2$.

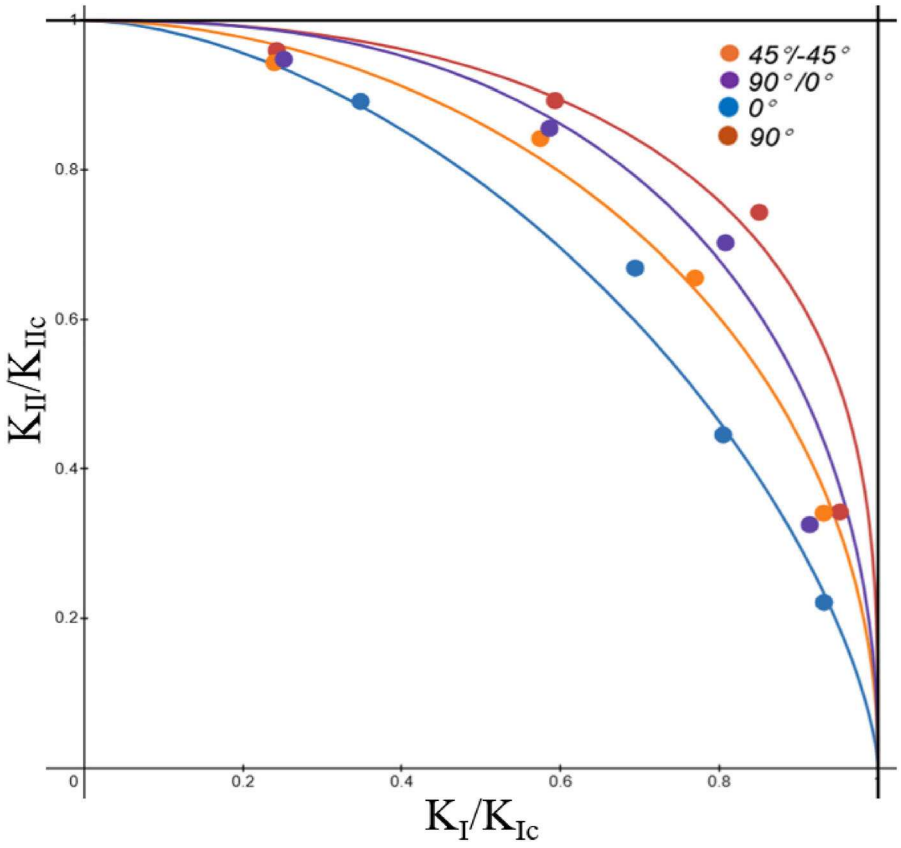

FIGURE 12 Mixed-mode fracture criterion for different printing orientations.

TABLE 3 Derived constants of the mixed-mode fracture criteria for different printing orientations.

Orientation	α	β
90°	2.3	3.3
45°/−45°	1.9	2.1
0°	1.7	1.5
90°/0°	2.5	2.2

The relatively higher α value indicates that the material in this direction is slightly more resistant to the openning mode compared to shearing mode.

In addition to the empirical constants (α and β), the area under each curve of the mixed-mode fracture criterion for each printing orientation provides additional significance. In general, the area beneath the curve represents the safe zone, indicating that cracks are less likely to initiate. Conversely, the area above the curve represents the unsafe zone, signifying that cracks will initiate and propagate. The graph reveals that the safe zone for the 90° orientation is overall larger than that of the other orientations because the crack propagation direction is perpendicular to the filament direction, which implies that more energy is necessary to break the filament. The safe zone for the 0° sample is the smallest since less fracture energy is required to initiate and propagate the cracks compared to the other orientations.

5 | CONCLUSIONS

In this study, an experimental investigation is performed to comprehend and quantify the fracture behavior of additively manufactured ABS with four different printing orientations under quasi-static mixed-mode conditions. The printing orientations played a significant role in pure mode-I and pure mode-II fracture toughness results, where the 90° printing orientation demonstrated the highest mode-I and mode-II fracture toughness compared to all other three orientations. The 0° printing orientation showed the lowest mode-I and mode-II fracture toughness. However, the pure mode-II fracture toughness of the 0° printing orientation is higher than that of pure mode-I, indicating higher fracture resistance to initiate the crack under pure mode-II conditions, as evidenced by a significant amount of shear zone ahead of the crack tip. The mixed-mode fracture criterion clearly demonstrates that the 90° printing orientation exhibits significant resistance to both opening and shearing modes compared to all other printing orientations. The empirical constants of the mixed-mode fracture criterion determined for all four

printing orientations are different, which provide insights on the dominance of the mode-I or mode-II component of fracture toughness on the initiation of the crack. The 0° printing orientation clearly demonstrated the least safe zone to initiate fracture compared to all other three orientations.

Overall, this study provides a comprehensive understanding of the mixed-mode fracture behavior of ABS. The developed mixed-mode criterion for FFF-printed ABS with different printing orientations can be complemented to determine the safety factors for applied complex loads when product design is based on fracture toughness, along with the traditional strength-based criterion. Moreover, the experimental outcomes and the proposed fracture criterion can be used to develop mixed-mode fracture models for finite element analysis and theoretical studies.

ACKNOWLEDGMENTS

The author greatly appreciates the financial support from the National Science Foundation grant # NSF-CMMI-2438062.

CONFLICT OF INTEREST STATEMENT

The authors declare that they have no known competing financial interests or personal relationships that could have appeared to influence the work reported in this paper.

DATA AVAILABILITY STATEMENT

Data Will be made available upon request.

ORCID

Vijaya B. Chalivendra https://orcid.org/0000-0002-7856-096X

REFERENCES

1. Chaudhary B, Li H, Ngwa AN, Matos H. Investigating the effects of coating systems on the degradation behavior of 3D-printed pressure vessels. *Mar Struct*. 2024;93:103540. doi:10.1016/j.marstruc.2023.103540
2. Chaudhary B, Li H, Matos H. Long-term mechanical performance of 3D printed thermoplastics in seawater environments. *Results Mater*. 2023;17:100381. doi:10.1016/j.rinma.2023.100381
3. Ahn SH, Montero M, Odell D, Roundy S, Wright PK. Anisotropic material properties of fused deposition modeling ABS. *Rapid Prototyp J*. 2002;8(4):248-257. doi:10.1108/13552540210441166
4. Guo N, Leu MC. Additive manufacturing: technology, applications and research needs. *Front Mech Eng*. 2013;8(3):215-243. doi:10.1007/s11465-013-0248-8
5. Popescu D, Zapciu A, Amza C, Baciu F, Marinescu R. FDM process parameters influence over the mechanical properties of polymer specimens: a review. *Polymer Test*. 2018;69:157-166. doi:10.1016/j.polymertesting.2018.05.020
6. Rezaeian P, Ayatollahi MR, Nabavi-Kivi A, Razavi N. Effect of printing speed on tensile and fracture behavior of ABS specimens produced by fused deposition modeling. *Eng Fract Mech*. 2022;266:108393. doi:10.1016/j.engfracmech.2022.108393
7. Uddin MS, Sidek M, Faizal M, Ghomashchi R, Pramanik A. Evaluating mechanical properties and failure mechanisms of fused deposition modeling acrylonitrile butadiene styrene parts. *J Manuf Sci Eng*. 2017;139(8):081018. doi:10.1115/1.4036713
8. Aliheidari N, Tripuraneni R, Ameli A, Nadimpalli S. Fracture resistance measurement of fused deposition modeling 3D printed polymers. *Polym Test*. 2017;60:94-101. doi:10.1016/j.polymertesting.2017.03.016
9. Chohan JS, Kumar R, Yadav A, et al. Optimization of FDM printing process parameters on surface finish, thickness, and outer dimension with ABS polymer specimens using Taguchi orthogonal Array and genetic algorithms. *Math Probl Eng*. 2022;2022:2698845. doi:10.1155/2022/2698845
10. Rajaee P, Ashenai Ghasemi F, Sajjadi SA, Fasihi M. Effect of raster angle on the fracture properties of additively manufactured ABS via essential work of fracture. *J Appl Polym Sci*. 2024;141(16):e55262. doi:10.1002/app.55262
11. Zhou YG, Zou JR, Wu HH, Xu BP. Balance between bonding and deposition during fused deposition modeling of polycarbonate and acrylonitrile-butadiene-styrene composites. *Polym Compos*. 2020;41(1):60-72. doi:10.1002/pc.25345
12. Cole DP, Riddick JC, Jaim HI, Strawhecker KE, Zander NE. Interfacial mechanical behavior of 3D printed ABS. *J Appl Polym Sci*. 2016;133(30):43671. doi:10.1002/app.43671
13. Li J, Yang S, Li D, Chalivendra V. Numerical and experimental studies of additively manufactured polymers for enhanced fracture properties. *Eng Fract Mech*. 2018;204:557-569. doi:10.1016/j.engfracmech.2018.11.001
14. Rabbi M, Chalivendra V, Li D. A novel approach to increase dynamic fracture toughness of additively manufactured polymer. *Exp Mech*. 2019;59(6):899-911. doi:10.1007/s11340-019-00486-3
15. Mclouth TD, Severino JV, Adams PM, Patel DN, Zaldivar RJ. The impact of print orientation and raster pattern on fracture toughness in additively manufactured ABS. *Addit Manuf*. 2017;18:103-109. doi:10.1016/j.addma.2017.09.003
16. Hart KR, Wetzel ED. Fracture behavior of additively manufactured acrylonitrile butadiene styrene (ABS) materials. *Eng Fract Mech*. 2017;177:1-13. doi:10.1016/j.engfracmech.2017.03.028
17. Knott JF. *Fundamentals of Fracture Mechanics*. Gruppo Italiano Frattura; 1973.
18. Vidakis N, Petousis M, Maniadi A, Koudoumas E, Liebscher M, Tzounis L. Mechanical properties of 3D-printed acrylonitrile-butadiene-styrene TiO(2) and ATO nanocomposites. *Polymers*. 2020;12:1589. doi:10.3390/polym12071589
19. Najimi M, Haji Aboutalebi F. Mixed mode crack initiation and propagation in functionally graded materials: experimental and numerical investigations. *Iran J Sci Technol Transact Mech Eng*. 2023;47(4):1829-1839. doi:10.1007/s40997-023-00591-8
20. Carpinteri A. *Fracture and Complexity: One Century since Griffith's Milestone*. Springer Nature; 2021.
21. Ayatollahi MR, Nabavi-Kivi A, Hosseini SS, Khosravani MR. Effect of nozzle diameter and raster orientation on tensile and fracture behavior of FDM-PLA specimens under mixed-

mode I/II loading. *Fatigue Fract Eng Mater Struct*. 2024;47(8): 2774-2788. doi:10.1111/ffe.14329

22. Ameri B, Taheri-Behrooz F, Majidi HR, Mohammad Aliha MR. Mixed-mode load bearing estimation of the cracked additively manufactured materials using stress/strain-based models. *Rapid Prototyp J*. 2023;29(2):218-231.
23. Ameri B, Taheri-Behrooz F. Advanced additive manufacturing of self-healing composites: Exploiting shape memory alloys for autonomous restoration under mixed-mode loading. *Mater Design*. 2023;234:112379.
24. Erdogan F, Sih G. On the crack extension in plates under plane loading and transverse shear. *J Basic Eng*. 1963;85(4):519-525. doi:10.1115/1.3656897
25. Hussain M, Pu S, Underwood J. *1973 National Symposium on Fracture Mechanics, Part II*. ASTM International; 1973.
26. Fakoor M, Khansari NM. General mixed mode I/II failure criterion for composite materials based on matrix fracture properties. *Theor Appl Fract Mec*. 2018;96:428-442. doi:10.1016/j.tafmec.2018.06.004
27. Ameri B, Taheri-Behrooz F, Aliha M. Fracture loads prediction of the modified 3D-printed ABS specimens under mixed-mode I/II loading. *Eng Fract Mech*. 2020;235:107181. doi:10.1016/j.engfracmech.2020.107181
28. Ameri B, Taheri-Behrooz F, Aliha M. Mixed-mode tensile/shear fracture of the additively manufactured components under dynamic and static loads. *Eng Fract Mech*. 2022;260:108185. doi:10.1016/j.engfracmech.2021.108185
29. Shahbaz S, Ayatollahi M, Petru M, Torabi A. U-notch fracture in additively manufactured ABS specimens under symmetric three-point bending. *Theoret Appl Fract Mech*. 2022;119: 103318. doi:10.1016/j.tafmec.2022.103318
30. Bahrami B, Ayatollahi MR, Sedighi I, Pérez MA, Garcia-Granada AA. The effect of in-plane layer orientation on mixed-mode I-II fracture behavior of 3D-printed polycarbonate specimens. *Eng Fract Mech*. 2020;231:107018. doi:10.1016/j.engfracmech.2020.107018
31. Nabavi-Kivi A, Ayatollahi MR, Rezaeian P, Razavi N. Investigating the effect of printing speed and mode mixity on the fracture behavior of FDM-ABS specimens. *Theor Appl Fract Mech*. 2022;118:103223. doi:10.1016/j.tafmec.2021.103223
32. Ameri B, Taheri-Behrooz F, Aliha M. Evaluation of the geometrical discontinuity effect on mixed-mode I/II fracture load of FDM 3D-printed parts. *Eng Fract Mech*. 2021;113:102953. doi:10.1016/j.tafmec.2021.102953
33. Syaefudin EA, Kholil A, Hakim M, Wulandari DA, Murtinugraha E. The effect of orientation on tensile strength 3D printing with ABS and PLA materials. *J Phys Conf Ser*. 2023;2596(1):012002.
34. Aliha M, Karimi HR, Ghoreishi S. Mixed-mode tensile/shear fracture of the additively manufactured components under dynamic and static loads. *Eng Fract Mech*. 2022;260:104425. doi:10.1016/j.engfracmech.2021.108185
35. Hua W, Li J, Zhu Z, et al. A review of mixed mode I-II fracture criteria and their applications in brittle or quasi-brittle fracture analysis. *Theoret Appl Fract Mech*. 2023;124:103741. doi:10.1016/j.tafmec.2022.103741
36. Suresh S, Shih C, Morrone A, O'dowd N. Mixed-mode fracture toughness of ceramic materials. *J Am Ceram Soc*. 1990;73(5): 1257-1267. doi:10.1111/j.1151-2916.1990.tb05189.x

How to cite this article: Leng Z, Li J, Chalivendra VB. Effect of printing orientation on mixed-mode fracture criterion of additively manufactured acrylonitrile butadiene styrene. *Polym Eng Sci*. 2025;65(6):2990-3004. doi:10.1002/pen.27193